1. Supporting Information :

1.2. Activation of Dolomite Flotation by Ferrous Hydroxide and Carbonate

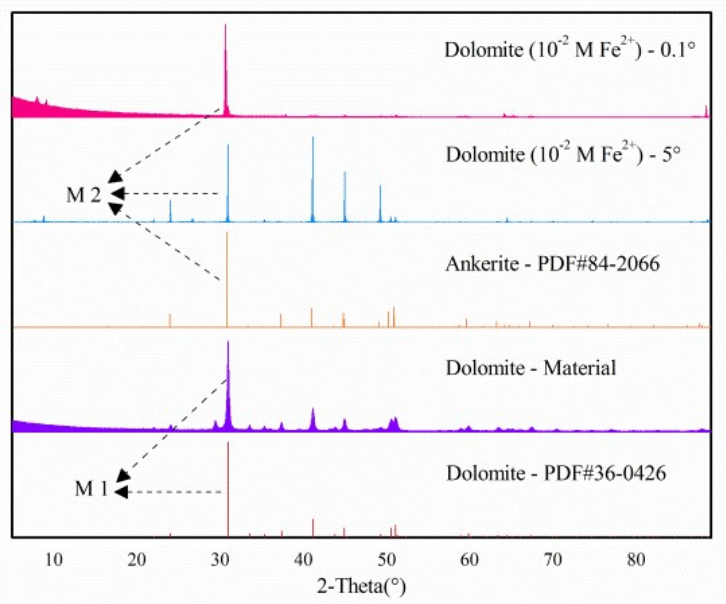


Figure S1. GI-XRD patterns of dolomite (M 1: Dolomite, M 2: Ankerite).

X-ray diffraction was performed at fixed incidence of 0.1° to enhance the signal arising from the sample surface (signals from the fixed incidence of 5° and traditional XRD (Dolomite-Material) were adopted as control group). Using a Rigaku Smartlab diffractometer with Cu Kα (9000 W) at 150 mA and 40 kV, we selected step sizes of 2° with time-by-step at 45 s over a 2θ range of 0.1° to 90°.

The GI-XRD results of dolomite treated with Fe^{2+} shows sharp metallic Fe peaks at 2θ positions 30.92, 41.12, 44.96 and 49.26° which corresponds to (104), (113), (202), and (024) of ankerite. These sharp metallic peaks revealed the presence of a Fe-rich species on the dolomite surface treated with Fe^{2+}.

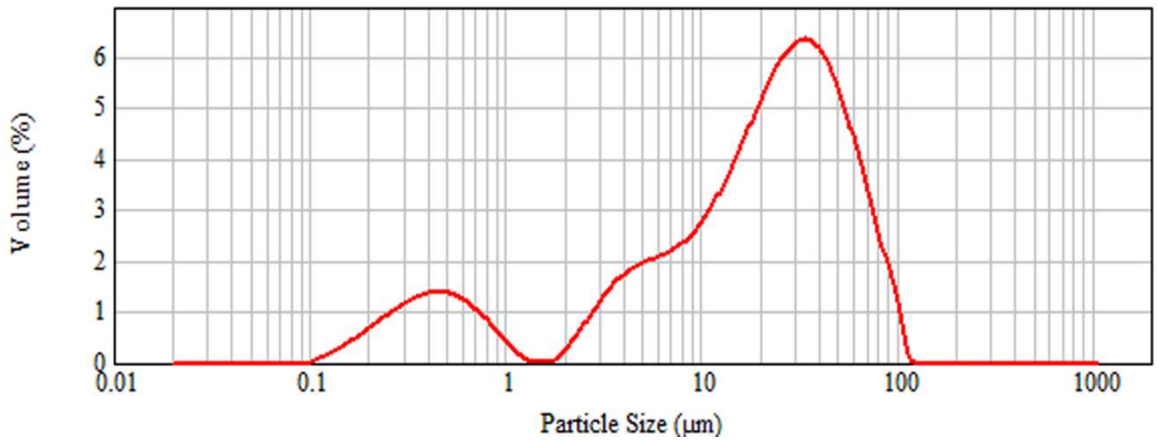


Figure S2. The size distribution of dolomite by laser particles analyzer (P90 = 60 μm).

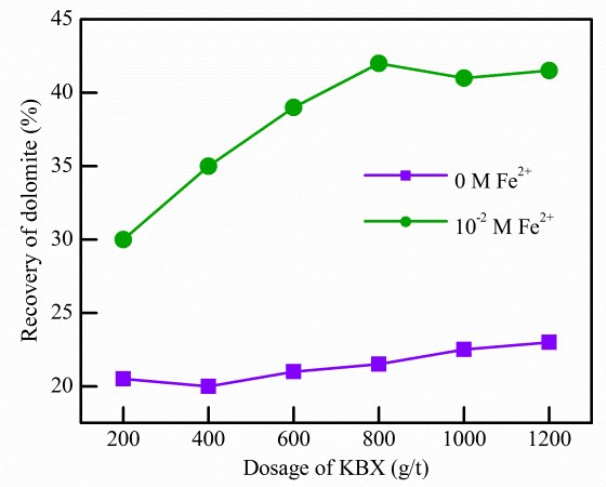


Figure S3. Effect of the SBX dosage on the modified dolomite recovery (pH=8.5).

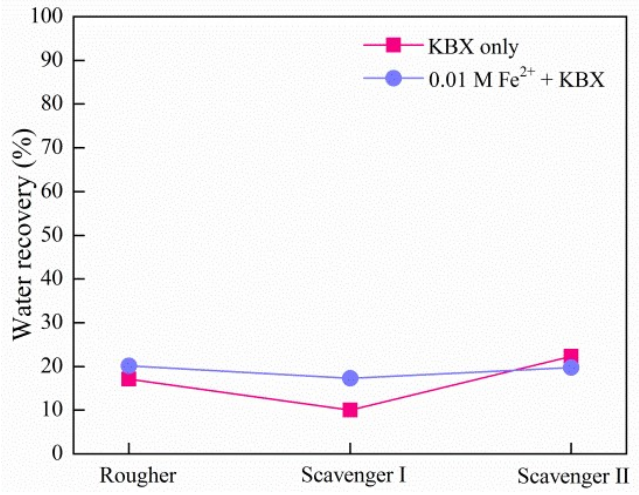


Figure S4. Water recovery in dolomite flotation tests (pH = 8.5).

The water recovery of dolomite with or without treated with Fe^{2+} is depicted in Figure S4. As expected, there is no obvious difference between the two samples, which is the most important evidence to declare that adding Fe^{2+} instead of the foam entrainment is responsible for the extra floatability of dolomite.

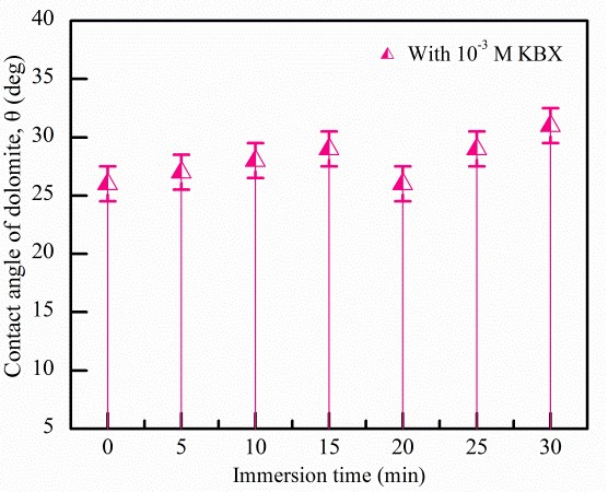


Figure S5. Contact angles of dolomite in xanthate-containing solutions with different immersion times (pH=8.5, c(SBX)=10^{-3} M).

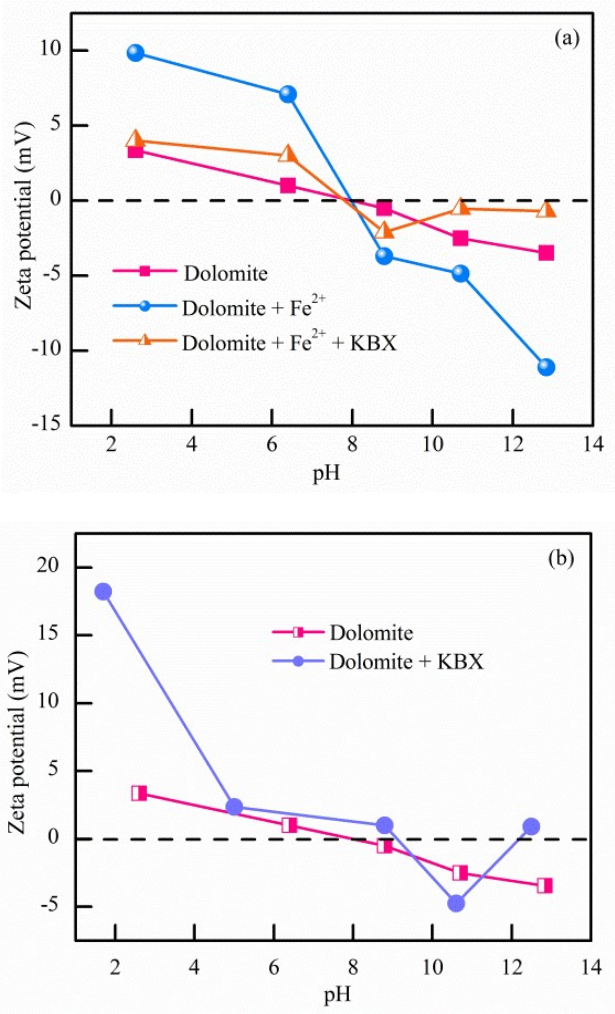


Figure S6. Zeta potential of dolomite under different reagent schemes (c(Fe^{2+}) = 10^{-3} M, c(SBX) = 10^{-3} M).

The zeta potential of dolomite was measured at 25℃ using Nano ZS manufactured by Malvern Instruments. 40 mg ground sample (-5 μm) combined with 40 ml distilled water was stirred for 1 min to obtain a good dispersion performance. HCl and NaOH solution were used to maintain the pH. 10^{-3} mol/L $FeSO_4$, and 10^{-3} mol/L SBX were added sequentially, with 3 mins stirring after each addition. The suspension was collected to take three measurements at each pH and the average values were reported.

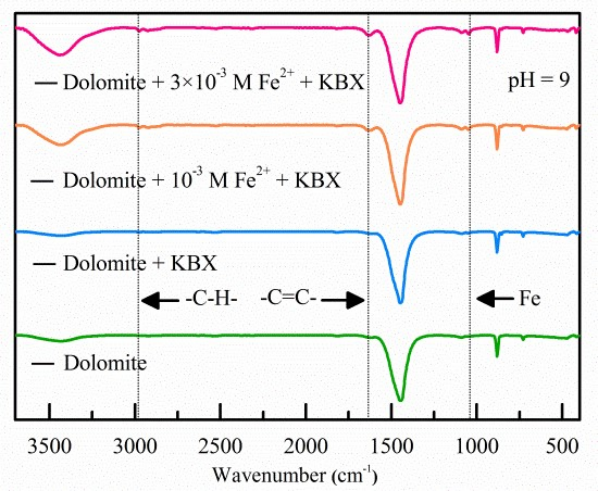


Figure S7. FTIR spectrum (400-3050cm^{-1}) of dolomite surface with different pretreatments (pH=8.5, c(SBX) = 10^{-3} M).

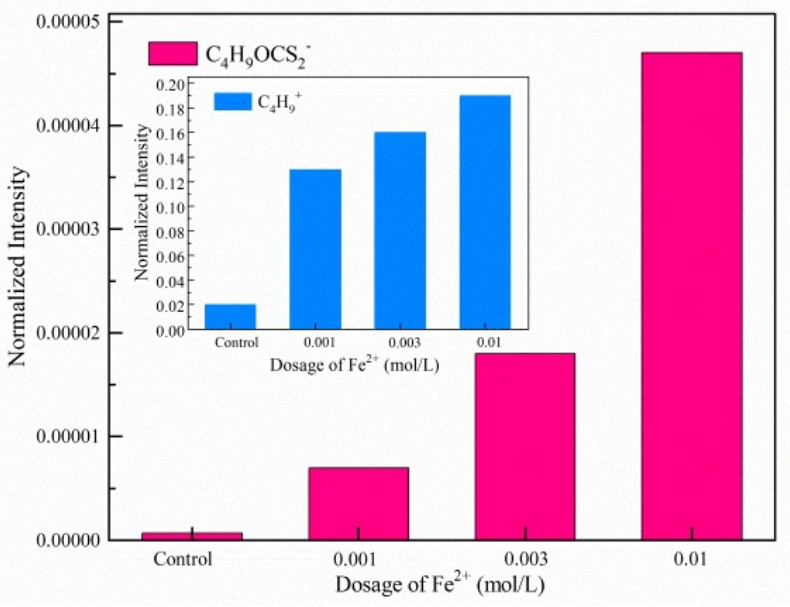


Figure S8. Accumulative normalized intensities of SBX adsorption on modified dolomite surface (pH=8.5, c(SBX) = 10^{-3} M).

The most significant diagnostic peak for SBX on the modified dolomite surface is $C_4H_9^+$ and $C_4H_9OCS_2^-$. As noted, the Fe^{2+} modified dolomite surface showed obviously higher accumulative normalized intensity than natural dolomite surface, indicating the stronger adsorption of SBX on modified dolomite surface, which is consistent with the flotation and thermodynamic results. The relevant mass spectra were summarized and submitted in Figure S9.

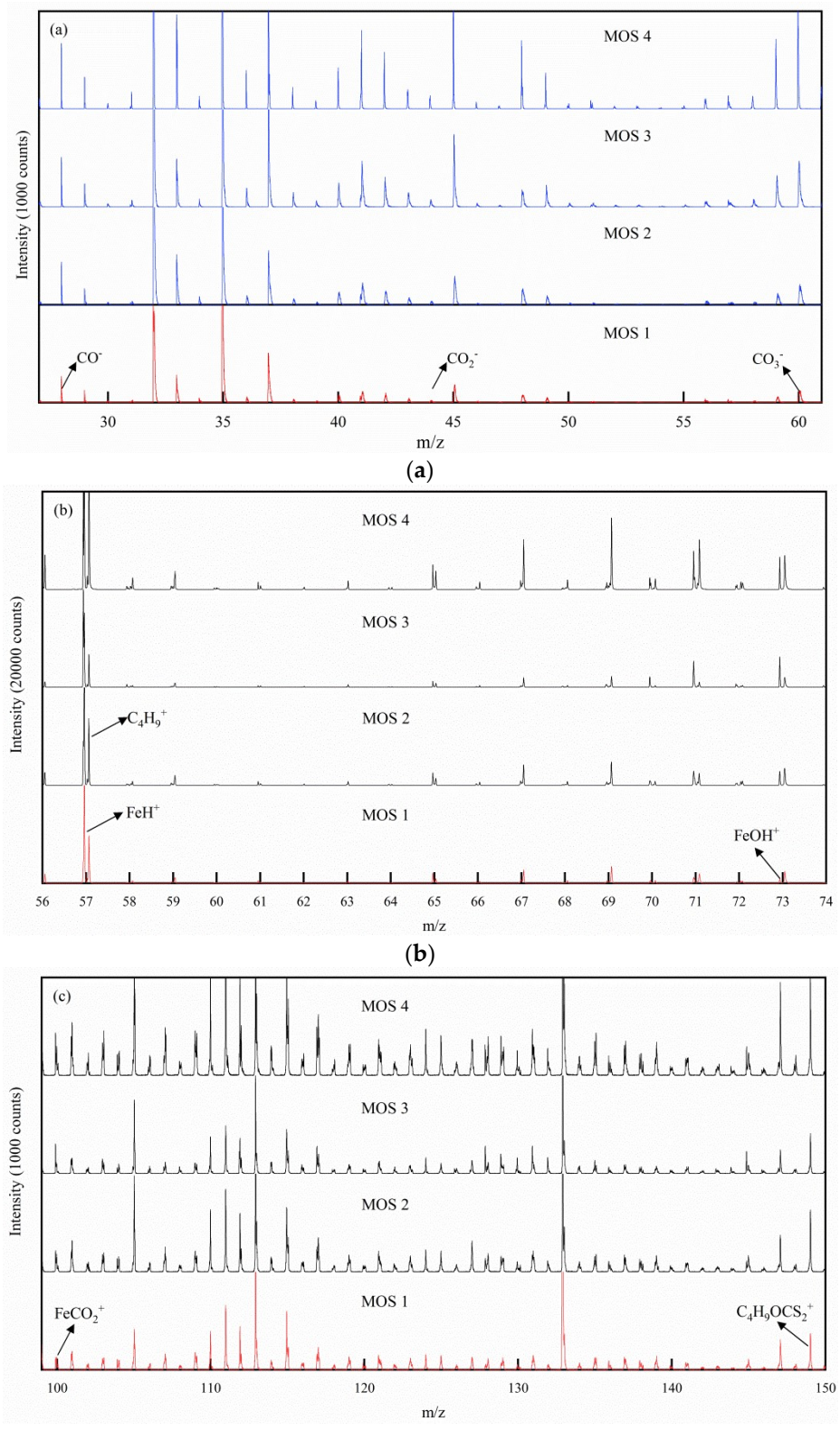


Figure S9. Negative secondary (**a**), and Positive secondary ion (**b**, **c**) mass spectra collected from the purity dolomite (MS 1), dolomite treated with 10^{-3} M Fe^{2+} and SBX (MS 2), dolomite treated with 3×10^{-3} M Fe^{2+} and SBX (MS 3), and dolomite treated with 10^{-2} M Fe^{2+} and SBX (MS 4) (pH=8.5, c(SBX) = 10^{-3} M).

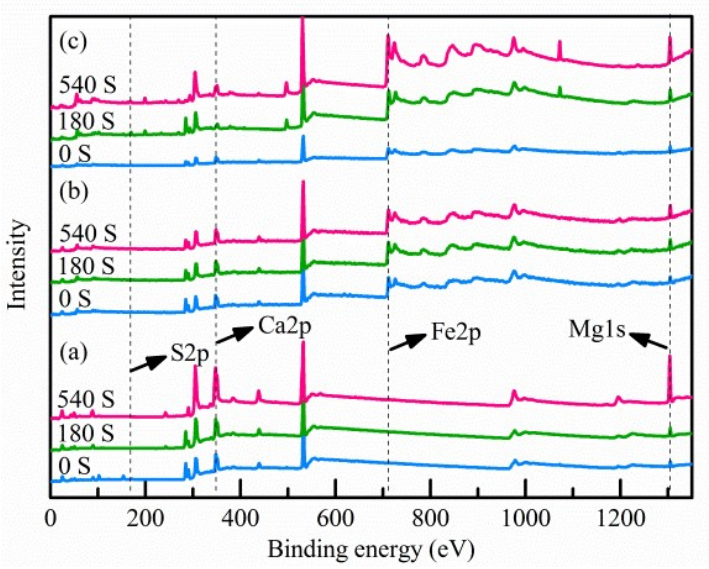


Figure S10. Full range XPS spectra of dolomite treated with 0 M Fe^{2+} (a), 10^{-3} M Fe^{2+} (b), and 10^{-2} M Fe^{2+} (c) as the function of etching time (pH=8.5, c(SBX)=10^{-3} M SBX).

Ar^{+} sputtering at 4 kV with different time was performed to acquire the depth profile of modified dolomite. Element proportion of the interested sample surface was expressed by the measurement values. For each sample of interest, data presented were normalized by the total atomic concentration.

The freshly polished dolomite surface was conditioned with different Fe^{2+} concentration, followed by the addition of SBX at the desired pH (adjusted by NaOH and HCl). Afterward, these samples were removed from the solution and dried with nitrogen. Then, the specimen was immediately introduced into the fore-vacuum chamber of the XPS instrument.

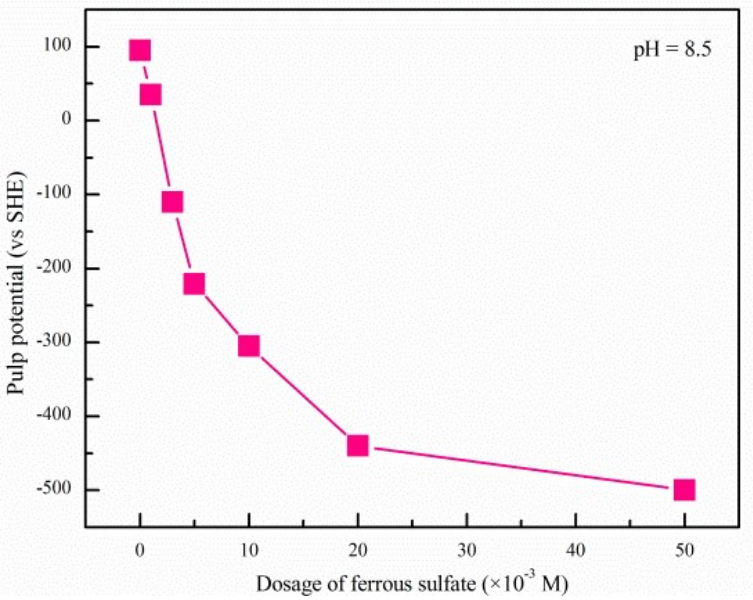
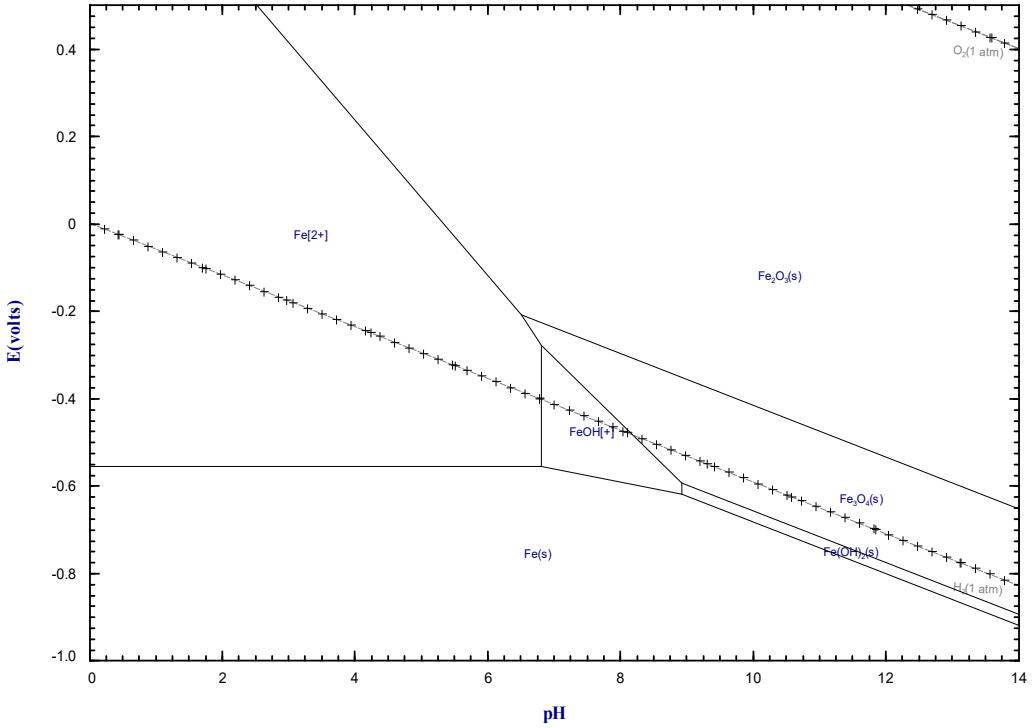
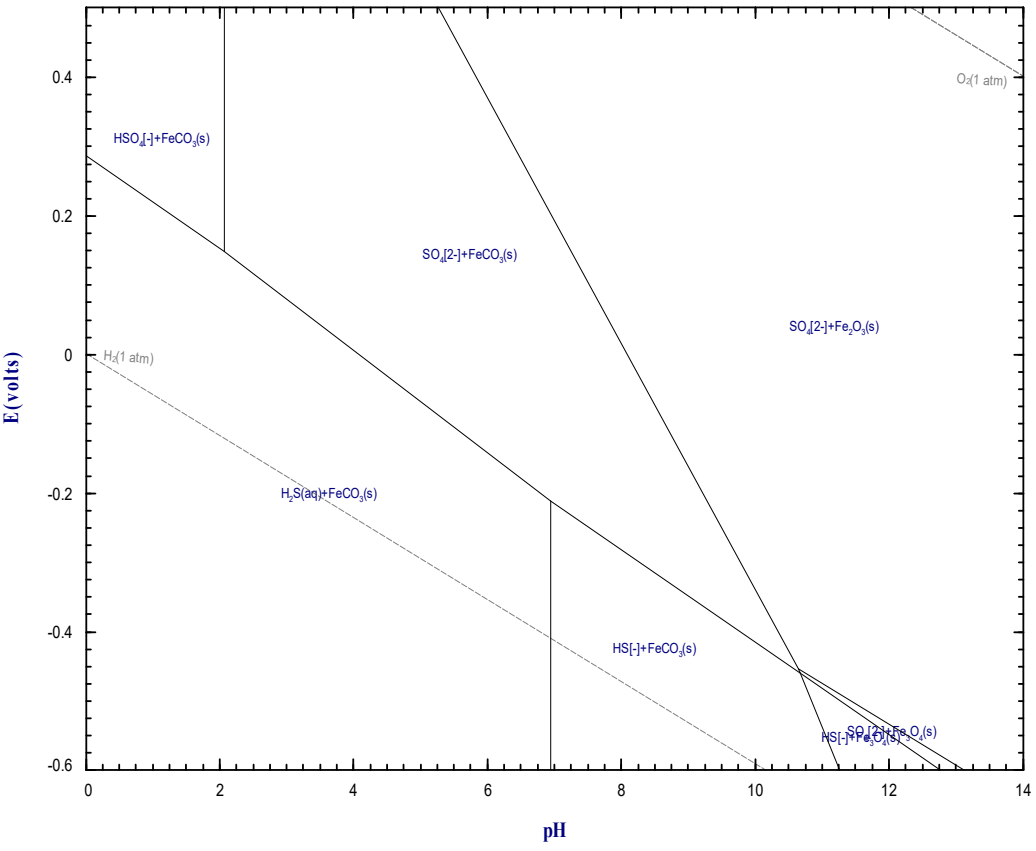


Figure S11. The pulp potential of modified dolomite as the Fe^{2+} dosage (pH=8.5, c(SBX)=10^{-3} M).



(**a**)



(**b**)

Figure S12. Eh-pH diagram of Fe-H_2O (a), and Fe-CO_3^{2-}-H2O system at 25℃ (Fe as the main element, the activities of dissolved Fe are assumed to be 1×10^{-5} M).



Figure S13. The picture of the dolomite pulp (pH=8.5, c(Fe^{2+})=10^{-2} M, c(SBX)=10^{-3} M).

The color of the pulp is celadon and remained stable without pumping the air, which is the contributory evidence of Fe^{2+} existed in the pulp. The existence of $Fe(OH)_2$ is well stated by the reversible reaction between $[Fe(H_2O)_6]^{2+}$ (which is stable in alkaline conditions) and $Fe(OH)_2$ [1]. Meanwhile, the existence of $FeCO_3$ was carefully depicted in Figure S12b.

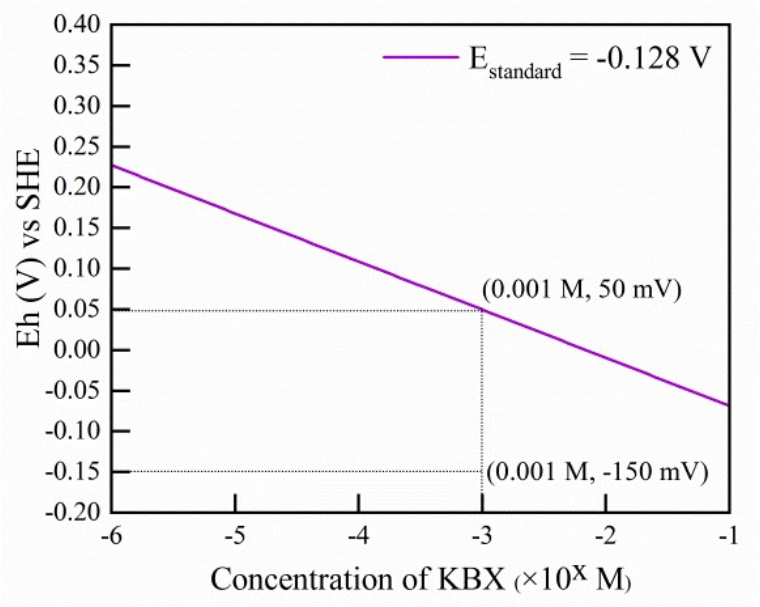


Figure S14. The calculated required potential for the xanthate oxidation under different concentration (pH=8.5).

The required potential for xanthate oxidation was calculated and referenced by the book of solution chemistry of flotation.

2.2. The Calculated D Electron Distribution of $Fe(OH)_2$ and $FeCO_3$

The first principle calculations are performed by Vienna Ab initio Simulation Package (VASP) with the projector augmented wave (PAW) method. The exchange-functional is treated using the Perdew-Burke-Ernzerhof (PBE) functional, in combination with the DFT-D correction. The calculations were performed in a spin-polarized manner. The cut-off energy of the plane-wave basis is set at 500 eV. The k-point sampling is performed with 4×4×4 Monkhorts-Packs. The self-consistent calculations apply a convergence energy threshold of 10^{-6} eV.

Table S1. Fe fitting parameters of MOS 1 (Normalise Chi Sqr: 0.097718, Abbe Criteria: 0.4524).

MOS 1	**Fe^{2+} 2p3**				**Fe^{3+} 2p3**			
BE, eV	706.3	707.2	708.3	709.3	710.2	711.3	712.5	713.7
FWHM, eV	1.35	1.59	1.40	1.51	1.41	1.35	1.55	1.60
% Area	1.2	2.0	3.7	16.6	23.0	23.5	20.0	10.0

Table S2. Fe fitting parameters of MOS 2 (Normalise Chi Sqr: 0.073817, Abbe Criteria: 0.5516).

MOS 2	**Fe^{2+} 2p3**				**Fe^{3+} 2p3**			
BE, eV	706.1	707.3	708.1	709.2	710.4	711.5	712.6	713.9
FWHM, eV	1.39	1.36	1.52	1.57	1.58	1.43	1.48	1.60
% Area	1.3	2.3	4.2	22.4	30.8	24.0	8.1	7.9

Table S3. Fe fitting parameters of MOS 3 (Normalise Chi Sqr: 0.13833, Abbe Criteria: 0.7367).

MOS 3	**Fe^{2+} 2p3**				**Fe^{3+} 2p3**			
BE, eV	706.2	707.1	708.1	709.2	710.3	711.5	712.7	713.8
FWHM, eV	1..7	1.39	1.42	1.50	1.50	1.46	1.52	1.61
% Area	3.3	2.8	11.4	26.9	18.2	17.7	12.6	7.1

Table S4. Fe fitting parameters of MOS 4 (Normalise Chi Sqr: 0.098671, Abbe Criteria: 0.4037).

MOS 4	**Fe^{2+} 2p3**				**Fe^{3+} 2p3**			
BE, eV	706.3	707.2	708.2	709.2	710.3	711.4	712.6	713.7
FWHM, eV	1.42	1.41	1.55	1.52	1.46	1.47	1.60	1.62
% Area	1.5	4.6	18.8	24.9	22.9	11.8	8.4	7.1

Table S5. O and C fitting parameters of MOS 1 (Normalise Chi Sqr: 0.38167, Abbe Criteria: 0.53).

Element	**O**				**C**		
MOS 1	O^{2-}	OH^-	Absorbed O	Other oxides	C-C	C-O	CO_3^{2-}
BE, eV	530.0	531.3	532.2	533.3	284.8	286.5	289.7
FWHM, eV	1.37	1.51	1.45	1.50	1.84	1.92	1.86
% Area	4.0	52.0	35.0	9.0	35.3	8.1	56.6

Table S6. O and C fitting parameters of MOS 2 (Normalise Chi Sqr: 0.36445, Abbe Criteria: 0.7361).

Element	**O**				**C**		
MOS 1	O^{2-}	OH^-	Absorbed O	Other oxides	C-C	C-O	CO_3^{2-}
BE, eV	530.2	531.3	532.2	533.1	284.8	286.7	289.8
FWHM, eV	1.49	1.55	1.42	1.69	1.90	1.90	1.83
% Area	6.0	48.0	36.0	10.0	43.4	7.6	49.0

Table S7. O and C fitting parameters of MOS 3 (Normalise Chi Sqr: 0.24233, Abbe Criteria: 0.2225).

Element	**O**				**C**		
MOS 1	O^{2-}	OH^{-}	Absorbed O	Other oxides	C-C	C-O	CO_3^{2-}
BE, eV	530.0	531.4	532.1	533.0	284.8	286.3	289.6
FWHM, eV	1.44	1.41	1.37	1.51	1.99	2.06	2.05
% Area	5.0	55.0	29.0	11.0	35.8	6.5	57.7

Table S8. O and C fitting parameters of MOS 4 (Normalise Chi Sqr: 0.36997, Abbe Criteria: 0.5004).

Element	**O**				**C**		
MOS 1	O^{2-}	OH^{-}	Absorbed O	Other oxides	C-C	C-O	CO_3^{2-}
BE, eV	530.1	531.3	532.1	533.2	284.8	286.6	289.7
FWHM, eV	1.60	1.42	1.39	1.56	1.70	1.80	1.68
% Area	6.0	38.0	45.0	11.0	44.7	5.2	50.1

References

1. Frolova L. Investigation of co-precipitation of Fe(II) and Ni(II) hydroxides. Mater Lett 2020;275:128065. Https://doi.org/10.1016/j.matlet.2020.128065.